Advances in Cochlear Implants
edited by I. J. Hochmair-Desoyer and E. S. Hochmair
Manz, Wien © 1994

Neural Membrane Model Responses To Sinusoidal Electrical Stimuli

T.T. Phan[1], M.W. White[1], C.C. Finley[2], L.A. Cartee[2]

[1]Department of Electrical and Computer Engineering, North Carolina State University, Box 7911, Raleigh, NC 27695

[2]Neuroscience Program Office, Research Triangle Institute, P.O. Box 12194, Research Triangle Park, NC 27709

Abstract — **To better understand psychophysical and neurophysiological responses to intracochlear electrical stimulation, the responses of three simple biophysical neural membrane models were investigated. We believe that several features of the psychophysical and neurophysiological responses may be attributable to the dynamics of the neural membrane. The three models under study were: the Hodgkin–Huxley model derived from experiments with squid axons, the Frankenhaeuser–Huxley model derived from experiments with toad nerve fibers, and the Chiu–et–al model derived from experiments with rabbit nerve fibers. Three comparative metrics were used: threshold, dynamic range, and latency of response. Threshold and dynamic range were measured as a function of sinusoidal stimulus frequency. Latency of response was measured as a function of sinusoidal stimulus amplitude. In addition to responses at 39 °C (an approximate temperature for mammals), the models' responses were also computed at 6, 16, and 29 °C to observe any temperature–dependent characteristics. Our results, based on the above metrics, show that: (1) all three studied neural membrane models exhibit dynamics that are correlated with features observed from human, monkey, and cat psychophysical and neurophysiological responses to intracochlear electrical stimulation, and (2) at the approximate temperature for mammals, the Hodgkin–Huxley model produces responses most similar to those from intracochlear electrical stimuli.**

I. INTRODUCTION

We believe that several features of the psychophysical and neurophysiological responses to intracochlear electrical stimulation may be attributable to the dynamics of the neural membrane. To better understand psychophysical and neurophysiological responses, the responses of three simple biophysical neural membrane models were investigated. This work extends earlier studies which model electrical stimulation of auditory fibers (Clopton et al., 1983; White, 1983; White, 1984; Colombo and Parkins, 1987; Motz and Rattay, 1986; Rattay and Motz, 1987). It is our hope that results from this study can be used to develop more accurate models and assist with initial decisions in future electrostimulation experiments. The three models under study were: the Hodgin–Huxley (HH) model derived from experiments with giant squid axons (Hodgin and Huxley, 1952), the Frankenhaeuser–Huxley (FH) model derived from experiments with toad myelinated nerve fibers (Frankenhaeuser and Huxley, 1964; Frankenhaeuser and Moore, 1963), and the Chiu–et–al (CRRS) model derived from experiments with rabbit myelinated nerve fibers (Chiu et al., 1979; Sweeney et al., 1987; Basser and Roth, 1991). Comparison between the models' responses and those from the electrical stimulations were based on three metrics: threshold contour (TC), dynamic range (DR), and latency response (LR). These three metrics, computed for each model at 39 °C, were compared to that exhibited in psychophysical and neurophysiological responses from humans, monkeys, and cats. In addition to 39 °C, an approximate temperature for mammals, the models' responses were also computed at 6, 16, and 29 °C to observe any temperature–dependent characteristics. In this paper, we will discuss a new action potential (AP) detection method for these membrane models, define the three comparative metrics, present our simulation results, and highlight key similarities and differences between the models and the electrical stimulations.

II. METHODS

A. Action Potential Detection

One major problem that single–node neural membrane modeling encounters is ensuring correct and consistent detection of AP's. Unlike in a multi–node model where an AP can propagate and the propagation can be precisely detected, an AP in a single–node membrane model may be viewed only as a membrane voltage "spike" and can often be falsely detected or ignored. The accuracy of the comparative metrics in this study strongly depends on correct and consistent detection of AP's in the simulations. In the initial phase of this study, three methods of detecting AP's were considered: visual inspection, voltage peak detection, and ion–gating tracking. The latter method, tracking the ion–gating events, was implemented because it was empirically found to be more reliable and consistent than the other two methods. In ion–gating tracking, a state machine tracks the membrane model's ionic gating events through the equations gating variables: n, m, and h for HH model; n, m, h, and p for FH model; and m and h for CRRS model. Figure 1 shows the AP detection state diagrams for the three models. An AP is detected whenever the state sequence A–B–A occurs. Detecting this inactive–active–inactivate sequence of transmembrane ionic fluxes that occur during the course of an AP, in turn, detects the occurring AP. Using the HH model as an example, the following text details this AP detection mechanism.

In Figure 1a for the HH model, when $m \leqq h$ (dominating Na inactivation), the membrane is in state A, indicating a subthreshold condition. When $m > h$ and $n < m$ (dominating Na activation), a transition from state A to state B occurs,

indicating the initiation of an AP. In state B, $m \geqq h$ indicates a continuing Na activation: the AP is in progress. When $m < h$ (re–domination of Na inactivation), a transition from state B back to state A occurs, indicating the termination of the AP and the restoration of the membrane to subthreshold. The ion–gating tracking method detects an AP by tracing the gating variables and recognizing the state sequence A–B–A. Even though all gating variables can be used in various relations to determine the state transitions, we found that those implemented appeared to ensure accurate detection of AP's. In the near future, we plan to investigate this AP detection method further by comparing it with the phase analysis technique of Dean and Lawrence (1983) and by using it to predict the initiation of propagating AP's in multi–node models. AP detection state diagrams for the FH and the CRRS models are shown in Figure 1b and 1c. AP detection for the FH model has the additional p gating variable to trace the activation of "non–specific ions." AP detection for the CRRS model only has Na activation and inactivation.

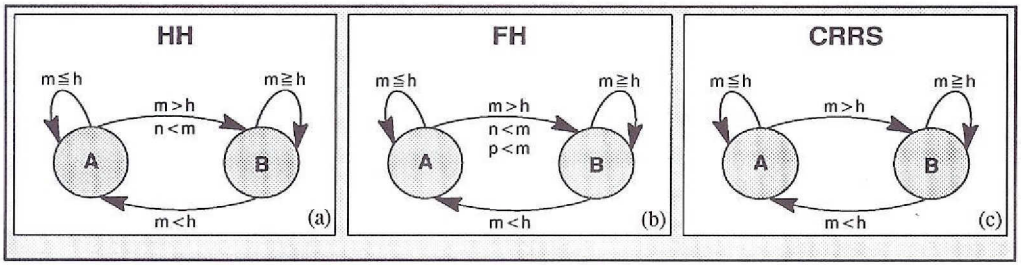

Figure 1: Ion–gating AP detection state diagrams for: (a) the HH model, (b) the FH model, and (c) the CRRS model. Gating variables are: m for Na activation, h for Na inactivation, n for K activation, and p for "non–specific ions" activation (Hodgin and Huxley, 1952; Frankenhaeuser and Huxley, 1964; Chiu et al., 1979).

B. Comparative Metrics Computation

In this study, the comparisons made between the models and the electrical stimulations were based on three metrics: threshold contour (TC), dynamic range (DR), and latency response (LR). Together, the three metrics characterize the membrane sensitivity: the TC provides the tuning information, the DR provides the range information, and the LR provides the timing information.

1) Threshold Contour

TC was obtained by plotting the threshold of AP activity as a function of stimulus frequency. The stimulus frequency is varied from 25 Hz to 25.6 Khz in 1 octave steps. For each stimulus frequency, the stimulus intensity (ie. the stimulus amplitude) is varied over an approximate 60 dB range, using an adaptive procedure that insured a minimum accuracy of 0.4 dB. At each stimulus frequency and intensity, a 10–cycle current train is injected into the model and the resulting membrane AP activity is recorded. The threshold of AP activity is defined as the stimulus intensity where the model first produces at least one AP in response to the 10–cycle stimulus train. The models' TC's are shown in Figure 2b and Figure 3.

2) Dynamic Range

DR was obtained by plotting the difference in stimulus intensity between threshold and saturation of AP activity as a function of stimulus frequency. The saturation of AP activity is defined as the stimulus intensity where the model first produces a maximal number of AP's in response to the 10–cycle stimulus train. Though not necessarily always 10, the maximal number of AP's of this value indicates the membrane's one–to–one response to the 10 stimulus cycles. To further ensure a correct determination of AP saturation, responses to increasing stimulus intensities to at least 12 dB above the observed AP saturation were also computed. The models DR's are shown in Figure 4b and Figure 5.

3) Latency Response

LR was obtained by plotting AP latency as a function of stimulus intensity. The AP latency is defined as the elapsed time from the onset of the stimulus cycle to the peak of the first AP. The elapsed time is extracted from period histograms of membrane AP activity in response to a 1–second stimulus duration. LR was computed at stimulus frequencies of 25, 50, 100, 200, and 400 Hz. At each frequency, the stimulus intensity was varied in 6 dB increments over a range of at least 25 dB above threshold. The models LR's are shown in Figure 6b and Figure 7. To simplify the comparison to existing electrical stimulation data, the axes of the LR have been transposed: AP latency on the abscissa and stimulus intensity on the ordinate. Latency is expressed as a percentage of stimulus period.

III. RESULTS AND DISCUSSION

A. Threshold Contour

Our comparisons of TC's are based on three sub–metrics: the TC minimum, the TC slope, and the "break" frequency. The TC minimum, defined as the lowest stimulus intensity on a TC, measures the maximal membrane sensitivity. For example, in Figure 2b, the TC minimum for the CRRS model is approximately –55 dB. The TC slope, defined as the maximum measured slope over one octave, approximates the degree of change in the membrane sensitivity. In Figure 2b, the TC slope for the CRRS model is approximately 15 dB/octave. The "break" frequency is defined as the frequency a) where the TC is at or near its minimum and b) at which the TC starts to break upward. The "break" frequency measures the tuning of membrane sensitivity. In Figure 2b, the "break" frequency for the CRRS model is approximately 1.6 KHz. The "break" frequency and the TC slope are used to compare characteristics of AP sensitivity between the models and the empirical measurements. The TC minimum is used to further identify temperature–dependent differences between the models.

At the approximate temperature for mammals, our study shows that even though all three models produce TC's qualitatively similar in shape to those from psychophysical experiments with monkey (Pfingst, 1989) and cat (Smith, 1992), the HH model's TC is most qualitatively similar. Figure 2a shows the animals' TC's. Figure 2b shows the models' TC's, computed at the approximate temperature for mammals. At this temperature, the HH model's TC exhibits a "break" frequency closest to those from the psychophysical experiments: 30 to 100 Hz from the monkey's and cat's data, 200 Hz from the HH model, 400 Hz from the FH model, and 1.6 KHz from the CRRS model. We also observe at this temperature that the TC slope from the HH model best fits the animals' data: 4 to 9 dB/octave for cats,

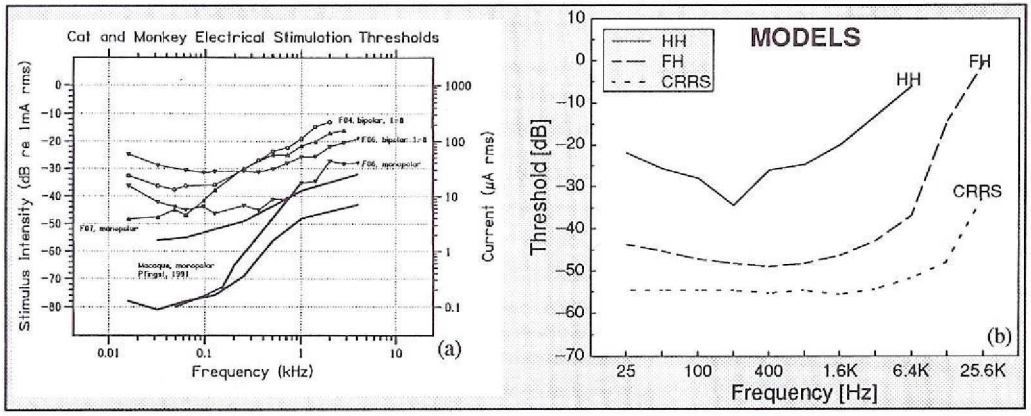

Figure 2: (a) TC's from the psychophysical responses of monkeys and cats (Smith, 1992). (b) TC's from the models' responses, computed at the approximate mammalian temperature of 39 °C. See legend in Figure 3 for the models' respective 0 dB reference stimulus levels.

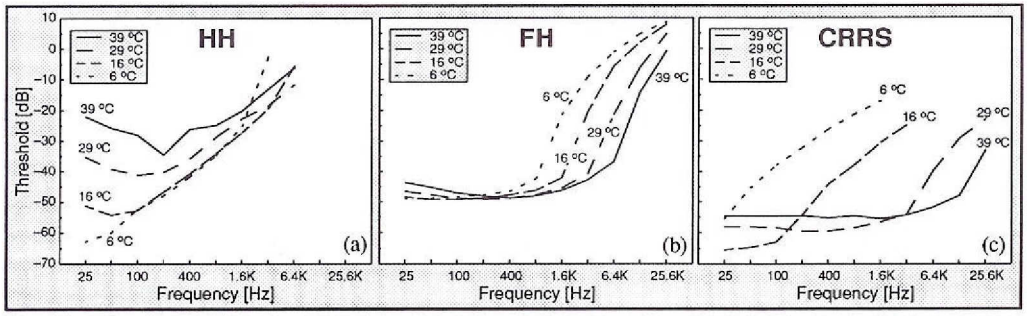

Figure 3: TC's computed at 6, 16, 29, and 39 °C from: (a) the HH model, (b) the FH model, and (c) the CRRS model. Dotted lines are TC's at 6 °C and solid lines are TC's at 39 °C. The 0 dB reference stimulus levels are: 1 mA for the HH and the CRRS models and 100 mA for the FH model.

6 to 13.5 dB/octave for monkeys, 8.4 dB/octave for the HH model, 22.6 dB/octave for the FH model, and 15 dB/octave for the CRRS model.

Figure 3 plots the models TC's at 6, 16, 29, and 39 °C. When computed at increasing temperature, the models' TC's exhibit increasing "break" frequencies ranging from: 25 to 200 Hz for the HH model, 50 to 400 Hz for the FH model, and 25 Hz to 1.6 KHz for the CRRS model. Also when computed at increasing temperature, each model produces different TC slope characteristics: generally decreasing from 22.7 down to 8.4 dB/octave for the HH model, relatively unchanged at 21 dB/octave with ±1 dB deviation for the FH model, and generally increasing from 10.1 to 15 dB/octave for the CRRS model. With increasing temperature, the TC's minima from the HH and the CRRS models increase while those from the FH model remain relatively flat.

B. Dynamic Range

At every simulated temperature, only the HH model produces DR's quantitatively similar to human psychophysical data (White, 1984). Figure 4a illustrates the human DR's. Figure 4b shows the models DR's, computed at the approximate temperature for mammals. The HH model and the data from humans exhibit greater DR at lower frequencies than at higher frequencies. An opposite trend is generally observed from both the FH and the CRRS models.

The study also shows that all three models exhibit a frequency around which each DR reaches a minimum. This frequency appears to correlate with the observed "break" frequency and, therefore, also increases with increasing

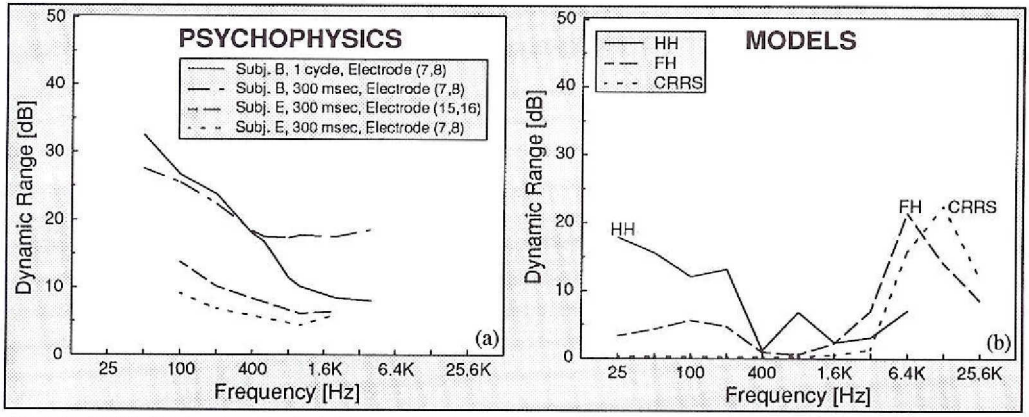

Figure 4: (a) DR's from human psychophysical data. (b) DR's from the models' responses, computed at the approximate mammalian temperature of 39 °C.

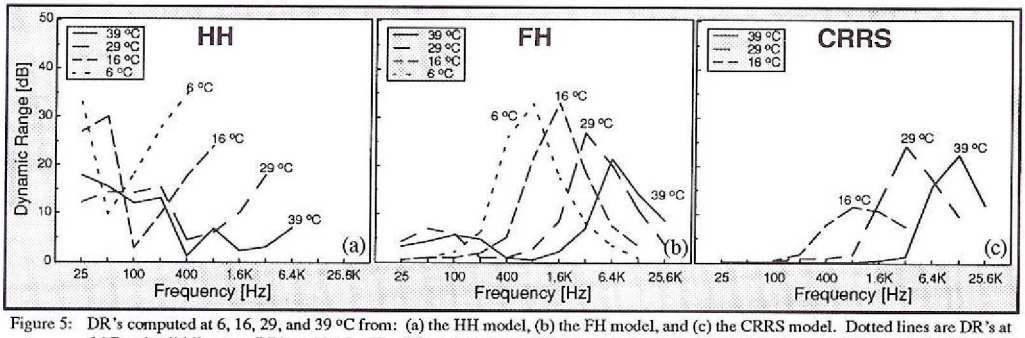

Figure 5: DR's computed at 6, 16, 29, and 39 °C from: (a) the HH model, (b) the FH model, and (c) the CRRS model. Dotted lines are DR's at 6 °C and solid lines are DR's at 39 °C. (The DR at 6 °C for the CRRS model has been omitted because we felt that results from our simulation were insufficient.)

temperature. Figure 5 plots the models DR's at 6, 16, 29, and 39 °C. Also with increasing temperature, the HH and the FH models show an overall decrease in their DR's. This decrease can be seen by the lowering of the peaks of the DR's as the temperature increases.

C. Latency Response

Our study shows that only the HH model produces LR's similar to those from electrical stimulation of cat's auditory nerve fibers (Van den Honert and Stypulkowski, 1987). Figure 6a shows the cats' LR's. Figure 6b shows the models' LR's, computed at the approximate temperature for mammals. LR's in Figures 6a and 6b were recorded in response to sinusoidal electrical stimulation at 100 Hz. The HH model and the data from cat show little change in the AP latency over a stimulus intensity range of 14 dB starting from threshold. The almost linear and vertical orientation of the LR's emphasize the independence of AP latency from stimulus intensity. LR's from the FH and the CRRS models, by comparison, rapidly decrease within the same 14 dB range.

When computed at increasing stimulus frequency from 25 to 400 Hz, the HH model exhibits profoundly increasing LR curves. Figure 7a shows the HH model LR's, computed at increasing stimulus frequency. The wide gap between the LR curves shows the latency changes with frequency. The much smaller gaps in Figures 7b and 7c show that LR's from the FH and the CRRS models have a smaller dependency on stimulus frequency. Results from electrical stimulations also show AP responses to either or both phases of the stimulus cycle while those from the models only have responses to the depolarizing phase. This phenomenon may be explained by the fact that the electrodes may be

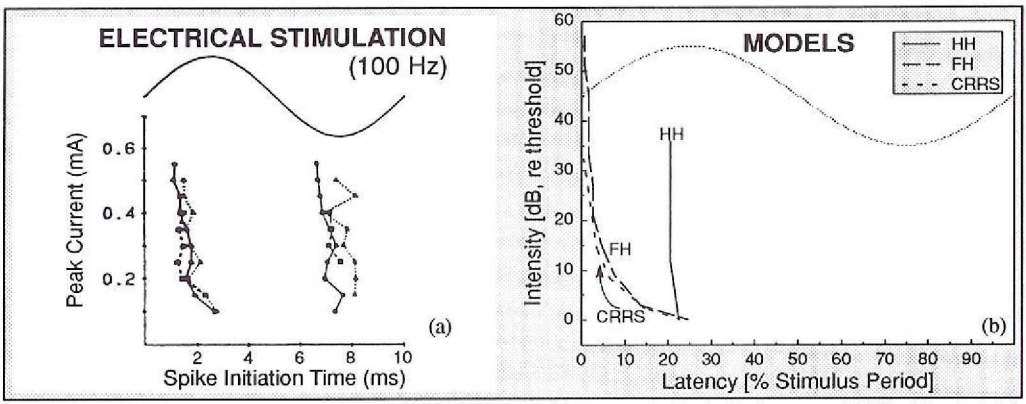

Figure 6: (a) LR's from cats neurophysiological data. (b) LR's from the models, computed with stimulus frequency of 100 Hz. The plot in (a) was extracted from Figure 7 of Van den Honert and Stypulkowski (1987).

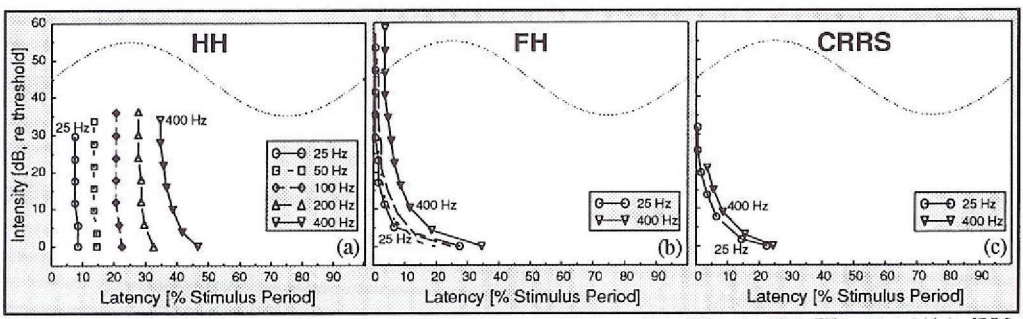

Figure 7: LR's computed with stimulus frequencies of 25, 50, 100, 200, and 400 Hz from: (a) the HH model, (b) the FH model, and (c) the CRRS model. Lines connecting inverted triangles are LR's in response to 400 Hz stimulus. Lines connecting circles are LR's in response to 25 Hz stimulus.

stimulating multiple nodes and recording the combined effects of these nodes. The studied models, on the other hand, only represent a single membrane patch.

IV. CONCLUSION

Results from our preliminary study show that all three neural membrane models exhibit dynamics that are correlated with features observed from psychophysical and neurophysiological responses to electrical stimulations. All three models produce TC's that are qualitatively similar in shape to those from electrical stimulations. Quantitatively similar TC slopes are observed for the HH model. At the approximate temperature for mammals, the HH model has a "break" frequency most similar to responses from monkeys and cats. The study also shows that only the HH model produces DR quantitatively similar to those from human psychophysical data. The HH model produces a greater DR at lower frequencies than at higher frequencies while the opposite trend is seen in the FH and the CRRS models. Finally, our study shows that only the HH model has LR's similar to those from cats' neurophysiological data. LR's from the HH model exhibit little dependency on stimulus intensity while those from the FH and the CRRS models exhibit a much greater dependency. At 39 °C, an approximate mammalian temperature, our study clearly shows that the HH model has responses most similar to data obtained from electrical stimulations.

It's surprising that the squid axon model appears to mimic auditory nerve behavior better than the other two models. The other two models were derived from species more like cat, monkey, and man. However, it is important to realize that we are just beginning to discover the diversity of nerve fibers *within* and *across* species. There can be large differences in the membrane dynamics of auditory fibers within the same species (Davis, 1993). From previous studies by this same author, there is evidence that different types of ion channels are present in different groups of auditory fibers *within the same animal*.

V. ACKNOWLEDGEMENTS

We thank Prof. D. Smith for his plot containing the combined cat and monkey psychophysical data. This work was partially supported by NIH, Program Project Grant 5 P01 DC00036–03.

VI. REFERENCES

Basser, P. J. and Roth, B. J. (1991). Stimulation of a myelinated nerve axon by electromagnetic induction. *Med. & Biol. Eng. & Comput.* **29**, 261–268.

Chiu, S. Y., Ritchie, J. M., Rogart, R. B., and Stagg, D. (1979) A quantitative description of membrane currents in rabbit myelinated nerve. *J. Physiol.* **292**, 149–166.

Clopton, B. M., Spelman, F. A., Glass, I., Pfingst, B. E., Miller, J. M., Lawrence, P. D., and Dean, D. P. (1983). Neural encoding of electrical signals. *Annals of NY Acad. of Sciences.* **405**, 146–158.

Colombo, J. and Parkins, C. W. (1987). A model of electrical excitation of the mammalian auditory nerve neuron. *Hearing Res.* **31**, 287–312.

Davis, R. L. (1993). Complex firing patterns of mouse 8th cranial nerve cells in vitro. Abstracts of the Sixth Midwinter Research Meeting of the Association for Research in Otolaryngology, St. Petersburg Beach, Florida.

Dean, D. and Lawrence, P. D. (1983). Application of phase analysis of the Frankenhaeuser–Huxley equations to determine threshold stimulus amplitudes. *IEEE Transaction on Biomedical Engineering*. BME–30, No. 12, 810–818.

Frankenhaeuser, B. and Huxley, A. F. (1964). The action potential in the myelinated nerve of *Xenopus laevis* as computed on the basis of voltage clamp data. *J. Physiol.* **171**, 302–315.

Frankenhaeuser, B. and Moore, L. E. (1963). The effect of temperature on the sodium and potassium permeability changes in myelinated nerve fibers of *Xenopus laevis*. *J. Physiol.* **169**, 431–437.

Hodgkin, A. L. and Huxley, A. F. (1952). A quantitative description of membrane current and its application to conduction and excitation in nerve. *J. Physiol.* **117**, 500–544.

Motz, H. and Rattay, F. (1986). A study of the application of the Hodgkin–Huxley and the Frankenhaeuser–Huxley model for electrostimulation of the acoustic nerve. *Neuroscience*. Vol. 18, No. 3, pp. 699–712.

Pfingst, B. E. (1989). Psychophysical constraints on biophysical/neural models of threshold. Cochlear Implants, edited by J. M. Miller and F. A. Spelman, pp. 161–185, 1989.

Rattay, F. and Motz, H. (1987). Simulation of a multichannel nerve array to pulse shapes produced by single channel electrostimulation. *Perception.* **16**, 769–776.

Smith, D. et al. (1992). Presentation from the Midwinter Research Meeting of the Association for Research in Otolaryngology, St. Petersburg Beach, Florida.

Sweeney, J. D., Mortimer, J. T., and Durand, D. (1987). Modeling of mammalian myelinated nerve for functional neuromuscular stimulation. *IEEE/Ninth Annual Conference of the Engineering in Medicine and Biology.*

Van den Honert, C. and Stypulkowski, P. H. (1987). Temporal response patterns of single auditory nerve fibers elicited by periodic electrical stimuli. *Hearing Research.* **29**, 207–222.

White, M. W. (1983). Electrical stimulation of the auditory nerve: Membrane models applied to the interpretation of psychophysical and electrophysiological response. Abstracts of the Sixth Midwinter Research Meeting of the Association for Research in Otolaryngology, St. Petersburg Beach, Florida.

White, M. W. (1984). Psychophysical and neurophysiological considerations in the design of a cochlear prosthesis. *Audiologia Italiana.* Vol. I – N. 2 – Aprile–Giugno, 77–117.